AD-A166 413 MITIGATION OF SCINTILLATION EFFECTS ON SPACE BASED RADARS THROUGH ADAPTIV..(U) MISSION RESEARCH CORP MONTEREY CA D L KNEPP ET AL. 30 APR 85 MRC/MTY-R-001 1/1

UNCLASSIFIED DNA-TR-85-174 DNA001-83-C-0021 F/G 17/9 NL

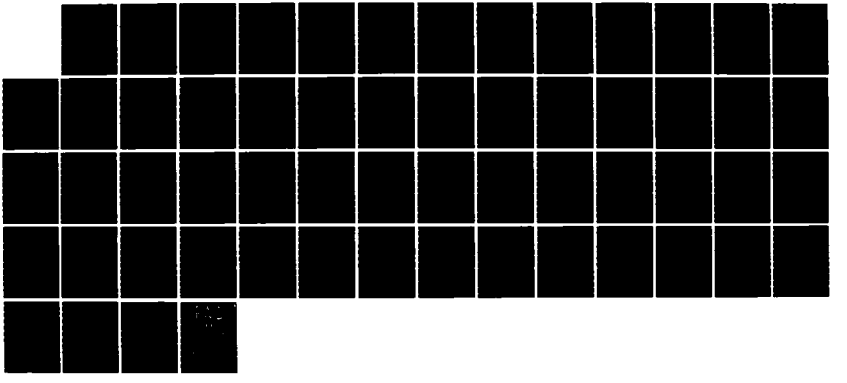

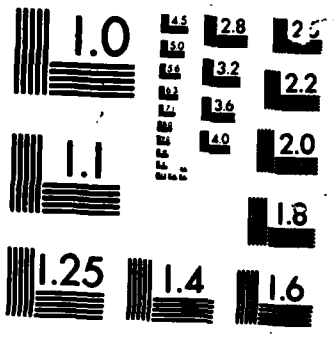

DNA-TR-85-174

MITIGATION OF SCINTILLATION EFFECTS ON SPACE BASED RADARS THROUGH ADAPTIVE NONCOHERENT PROCESSING

Dennis L. Knepp
William L. Bradford
Mission Research Corporation
2300 Garden Road, Suite #2
Monterey, CA 93940

30 April 1985

Technical Report

CONTRACT No. DNA 001-83-C-0021

THIS WORK WAS SPONSORED BY THE DEFENSE NUCLEAR AGENCY
UNDER RDT&E RMSS CODE B322084466 S99QMXBA00007 H2590D.

Prepared for
Director
DEFENSE NUCLEAR AGENCY
Washington, DC 20305-1000

DISTRIBUTION LIST UPDATE

This mailer is provided to enable DNA to maintain current distribution lists for reports. We would appreciate your providing the requested information.

☐ Add the individual listed to your distribution list.

☐ Delete the cited organization/individual.

☐ Change of address.

NAME: _____

ORGANIZATION: _____

OLD ADDRESS	CURRENT ADDRESS
_____	_____
_____	_____
_____	_____

TELEPHONE NUMBER: ( ) _____

SUBJECT AREA(s) OF INTEREST:

_____	_____
_____	_____
_____	_____

DNA OR OTHER GOVERNMENT CONTRACT NUMBER: _____

CERTIFICATION OF NEED-TO-KNOW BY GOVERNMENT SPONSOR (if other than DNA):

SPONSORING ORGANIZATION: _____

CONTRACTING OFFICER OR REPRESENTATIVE: _____

SIGNATURE: _____

UNCLASSIFIED
SECURITY CLASSIFICATION OF THIS PAGE

AD-A166 413

REPORT DOCUMENTATION PAGE

1a REPORT SECURITY CLASSIFICATION UNCLASSIFIED	1b RESTRICTIVE MARKINGS
2a SECURITY CLASSIFICATION AUTHORITY N/A since Unclassified	3 DISTRIBUTION / AVAILABILITY OF REPORT Approved for public release; distribution is unlimited.
2b DECLASSIFICATION / DOWNGRADING SCHEDULE N/A since Unclassified	
4 PERFORMING ORGANIZATION REPORT NUMBER(S) MRC/MTY-R-001	5 MONITORING ORGANIZATION REPORT NUMBER(S) DNA-TR-85-174
6a NAME OF PERFORMING ORGANIZATION Mission Research Corporation 6b OFFICE SYMBOL (If applicable)	7a NAME OF MONITORING ORGANIZATION Director Defense Nuclear Agency
6c ADDRESS (City, State, and ZIP Code) 2300 Garden Road, Suite #2 Monterey, CA 93940	7b ADDRESS (City, State, and ZIP Code) Washington, DC 20305-1000
8a NAME OF FUNDING / SPONSORING ORGANIZATION 8b OFFICE SYMBOL (If applicable)	9 PROCUREMENT INSTRUMENT IDENTIFICATION NUMBER DNA 001-83-C-0021
8c ADDRESS (City, State, and ZIP Code)	10 SOURCE OF FUNDING NUMBERS PROGRAM ELEMENT NO: 62715H; PROJECT NO: S99QMXB; TASK NO: A; WORK UNIT ACCESSION NO: DH007947

11 TITLE (Include Security Classification)
MITIGATION OF SCINTILLATION EFFECTS ON SPACE BASED RADARS THROUGH ADAPTIVE NONCOHERENT PROCESSING

12 PERSONAL AUTHOR(S)
Knepp, Dennis L. and Bradford, William L.

13a TYPE OF REPORT	13b TIME COVERED	14 DATE OF REPORT (Year, Month, Day)	15 PAGE COUNT
Technical	FROM 831201 TO 850429	850430	58

16 SUPPLEMENTARY NOTATION
This work was sponsored by the Defense Nuclear Agency under RDT&E RMSS Code B322084466 S99QMXBA00007 H2590D.

17 COSATI CODES			18 SUBJECT TERMS (Continue on reverse if necessary and identify by block number)
FIELD	GROUP	SUB-GROUP	
17	9		Space Based Radar, Random Media, Signal Scintillation, Radar Performance, Ionospheric Propagation,
20	14		

19 ABSTRACT (Continue on reverse if necessary and identify by block number)

A space based radar system must deal with potential operating environments in which the propagation paths are severely disturbed, resulting in fast fading of signals and diminished detection and tracking performance. Part of an ongoing effort to design a system which can optimize performance in such an environment has focussed on the use of noncoherent integration of multiple coherent dwells in a scan. This report investigates the possibility that if knowledge of the fading rate were available, the radar could benefit by using an adaptive processing strategy to improve detection performance.

20 DISTRIBUTION / AVAILABILITY OF ABSTRACT ☐ UNCLASSIFIED/UNLIMITED ☒ SAME AS RPT ☐ DTIC USERS	21 ABSTRACT SECURITY CLASSIFICATION UNCLASSIFIED
22a NAME OF RESPONSIBLE INDIVIDUAL Betty L. Fox	22b TELEPHONE (Include Area Code) (202) 325-7042 22c OFFICE SYMBOL DNA/STTI

DD FORM 1473, 84 MAR 83 APR edition may be used until exhausted
All other editions are obsolete

SECURITY CLASSIFICATION OF THIS PAGE
UNCLASSIFIED

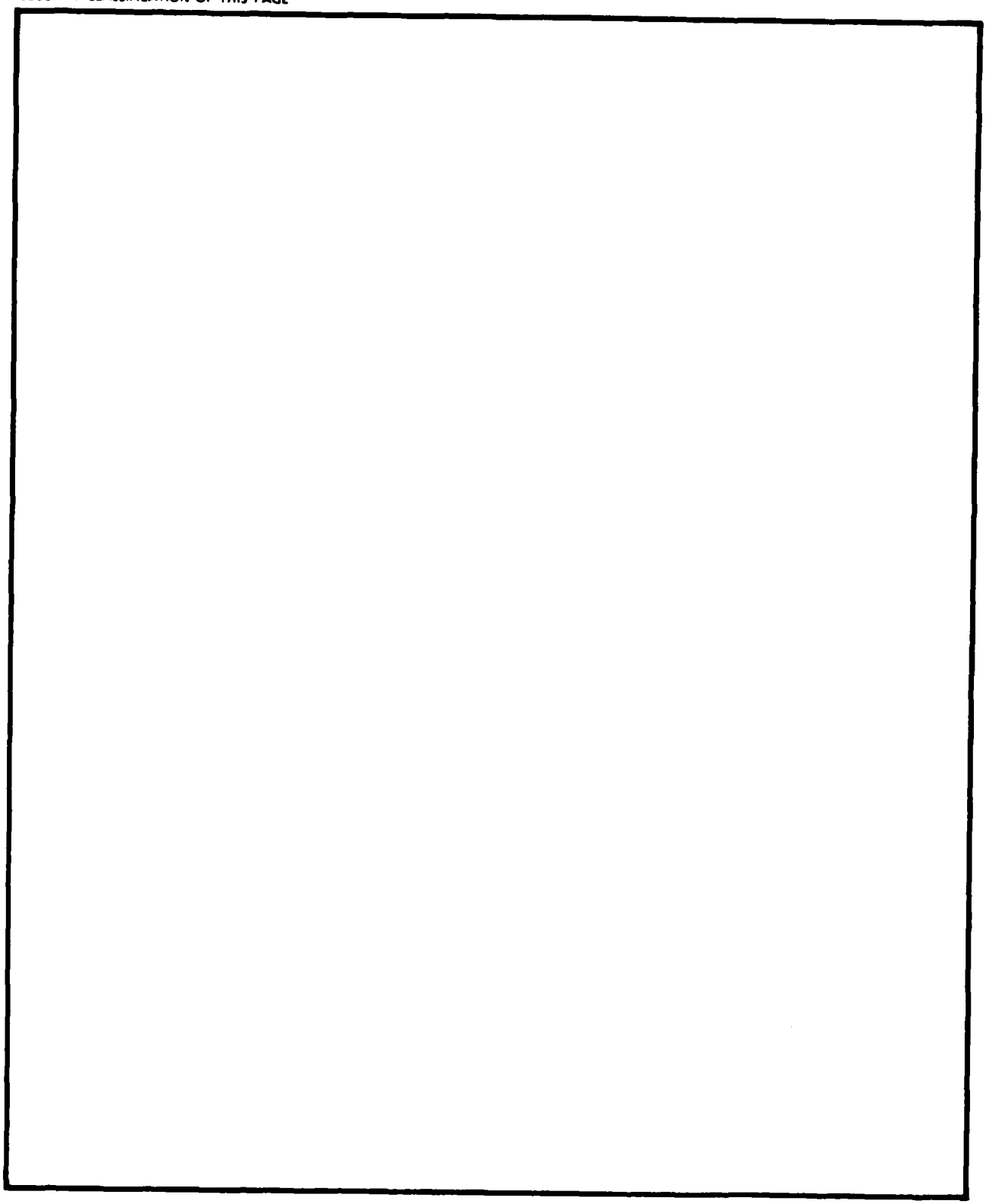

TABLE OF CONTENTS

LIST OF ILLUSTRATIONS

LIST OF ILLUSTRATIONS (Continued)

LIST OF ILLUSTRATIONS (Concluded)

LIST OF TABLES

LIST OF TABLES (Concluded)

SECTION 1

INTRODUCTION

The performance of a space based radar (SBR) is highly dependent upon the characteristics of the propagation channel through the ionosphere, since even small fluctuations in received power can result in degradation. Spatial irregularities in the electron density in the ionosphere can produce rapid random fluctuations in the amplitude, phase, and angle-of-arrival of propagating electromagnetic waves. These fluctuations, called scintillation, have been observed in VHF and UHF satellite communication links operating through the ambient ionosphere (Pope and Fritz, 1971; Skinner et al., 1971; Taur, 1976; Fremouw et al, 1978). Strong scintillation has occasionally been observed at frequencies as high as L-Band. To increase survivability the effects of signal fluctuations due to propagation through disturbed ionospheric channels should be considered in the initial stages of SBR design.

In a highly disturbed propagation environment, the scintillation in the amplitude of a signal may be described by Rayleigh amplitude statistics. Such conditions are likely to apply after high altitude nuclear explosions (Arendt and Soicher, 1964; King and Fleming, 1980), or after chemical releases (Davis et al., 1974; Wolcott et al., 1978). Increased electron densities and irregularities in ionization structure can lead to intense Rayleigh signal scintillation at frequencies as high as the 7-8 GHz SHF band (Knepp, 1977). An SBR using UHF to SHF, with the potential to operate in highly disturbed environments, must be designed with the

effects of scintillation in mind.

Earlier work (Knepp and Dana, 1982, 1983), investigated the performance of a space based radar operating in an environment characterized by a severely disturbed propagation channel. It was shown that strong scintillation causes severe degradation in detection performance. In particular, systems relying upon coherent integration of many pulses are susceptible to fast fading, which can dramatically reduce SBR detection performance.

In this report an inverse measure of scintillation severity is used, namely the signal decorrelation time, τ_0. Large values of τ_0 correspond to slow fading conditions, while small values of τ_0 indicate fast fading. Under fast fading conditions, the signal decorrelation time is small with respect to the coherent processing time so that the coherent integration process experiences a loss relative to its performance under slow fading conditions. This loss is caused by the destructive addition of successive radar pulses which are uncorrelated in amplitude and phase. The average received power at the output of the integrator is then reduced. Figure 1 shows the coherent integration loss, which is the ratio of the power out of the integrator with no fading to the power out of the integrator with fading.

As the signal decorrelation time decreases, the relative power output of the integrator decreases. If a scan, consisting of relatively large number of pulses (on the order of 100-500), is divided into dwells or bursts, over which the coherent integration takes place, the coherent integration loss will be reduced. By noncoherently adding the power from each dwell, the signal output per

scan is expected to be improved over the output of a scan which has not been subdivided into dwells.

The purpose of work reported here is to determine the trade-offs involved in a scheme which adaptively varies the number of coherent integration processes (dwells) within a scan. It will be shown that some improvement in performance is available if such a scheme is adopted, but that some increased complexity in the design of a space based radar is required.

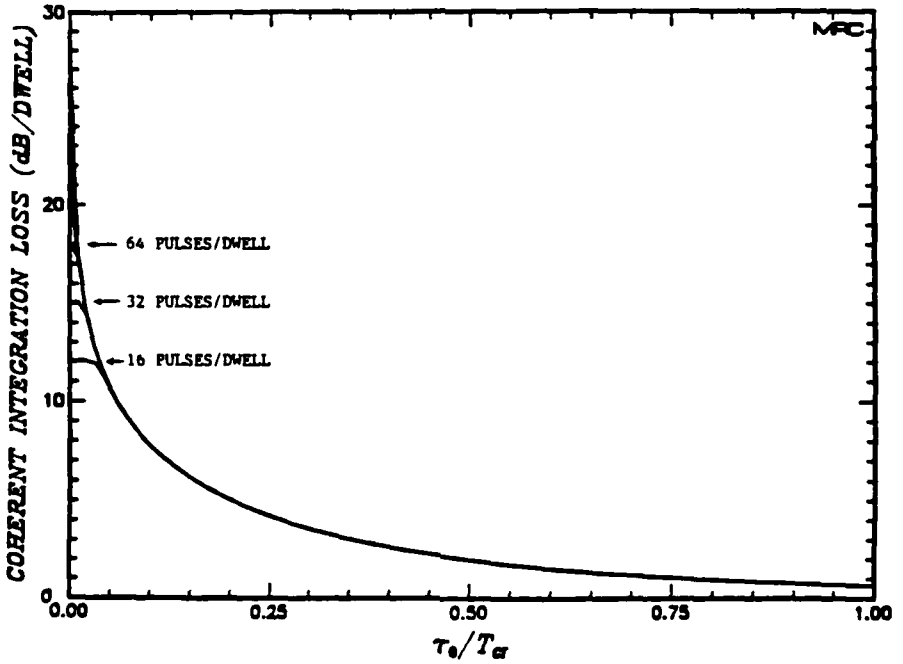

Figure 1. Effect of finite number of pulses per dwell on coherent integration loss.

SECTION 2

RECEIVED SIGNAL STATISTICS

In this report it is assumed that a space based radar must operate in an environment where the one-way signal propagation channel is so disturbed that the channel output signal is described with Rayleigh amplitude statistics. That is, a transmitted signal with constant amplitude will be received with amplitude fluctuations with first order statistics corresponding to a Rayleigh probability density function. Rayleigh statistics are worst case statistics, in the sense that no matter how much worse the disturbance becomes, the received signal does not deviate from the worst case Rayleigh probability distribution. This is true for the propagation of electromagnetic signals over a wide frequency range in many different kinds of random media including laser propagation in turbulent air (Fante, 1975; Goodman, 1976), VHF propagation through the ionosphere (Fremouw et al, 1978), and through striations composed of barium ions (Marshall, 1978). For propagation channels disturbed by high altitude nuclear bursts, Rayleigh statistics describe the signal fading characteristics (Wittwer, 1980).

RECEIVED SIGNAL FIRST-ORDER STATISTICS

Any actual received radar signal power, S_r, may be expressed as

$$S_r = S_0[C/\langle C\rangle]S \qquad (1)$$

where S_0 is the mean power returned by a point target and S is the fractional change in the power due to the the propagation channel. The effect of a fluctuating target cross section, C, is also included, normalized to the mean target cross section, <C>. The mean signal level is contained within the factor S_0, so that <S> may be set to unity. In this formulation, received signal fluctuations are due both to the fluctuations in target cross section and to fluctuations caused by the disturbed propagation channel.

TARGET STATISTICS

In this report the statistics which describe fluctuations in target cross section are assumed to be those applying to a Swerling type 2 target. That is, the target cross section varies independently from dwell to dwell, but is constant for all the pulses comprising the coherent dwell. The radar cross section, C, obeys an exponential probability distribution

$$p(C) = (1/\langle C\rangle)\exp(-C/\langle C\rangle) \qquad (2)$$

where <C> is the mean cross section. Equation 2 fully describes the first order statistics of the target cross section. To complete the description of the first order statistics of the received power, the specification of the first order fluctuations due to the disturbed propagation channel are required.

PROPAGATION CHANNEL STATISTICS

For monostatic SBR operation, the transmitted and received signals traverse the same path, so that the irregularities in the intervening medium are identical for both. In this case, the received voltage is proportional to the square of the voltage for one-way propagation. The received power is similarly proportional to the square of the received power after one-way propagation. The two-way or monostatic probability distribution for received power is then given by (Knepp and Dana, 1983)

$$p_m(S) = \frac{1}{\sqrt{2S\langle S\rangle}} \exp\{-\sqrt{2S/\langle S\rangle}\} \qquad (3)$$

where <S> is the mean received power.

The combined effect of fluctuations in the propagation channel and target cross section is obtained by multiplying the two probability density functions. The resulting function can then be used to obtain the cumulative probability function, which provides a means of assessing the probability of occurence of deep fades, which are detrimental to radar performance. The cumulative distribution for the received power, S_r, in the monstatic case is given by

$$P_m(S_r) = 1 - \int_0^{\infty} \exp\{-u-2S_r/(u^2S_0)\}du \qquad (4)$$

where S_r is the received power and S_0 is the mean received power.

Figure 2 shows the cumulative probability functions for the combined Swerling 2 target and monostatic radar propagation channel. For comparison, the figure also shows the cumulative probability

distributions for three other cases. The curve marked "no fading" applies to the Swerling 2 target with a constant (non-fluctuating) propagation channel. The curve marked "one-way fading" applies to the bistatic radar case where one of the one-way propagation paths is undisturbed. The remaining curve, marked "bistatic radar" applies to the case of a bistatic radar where both one-way propagation channels exhibit Rayleigh fluctuations. The distinction between monostatic and the bistatic curves is that, in the monostatic case, the electromagnetic wave propagates through the same irregularities on each of the two one-way propagation paths. In the bistatic radar case, the two one-way paths are independent, giving the statistics shown in the figure.

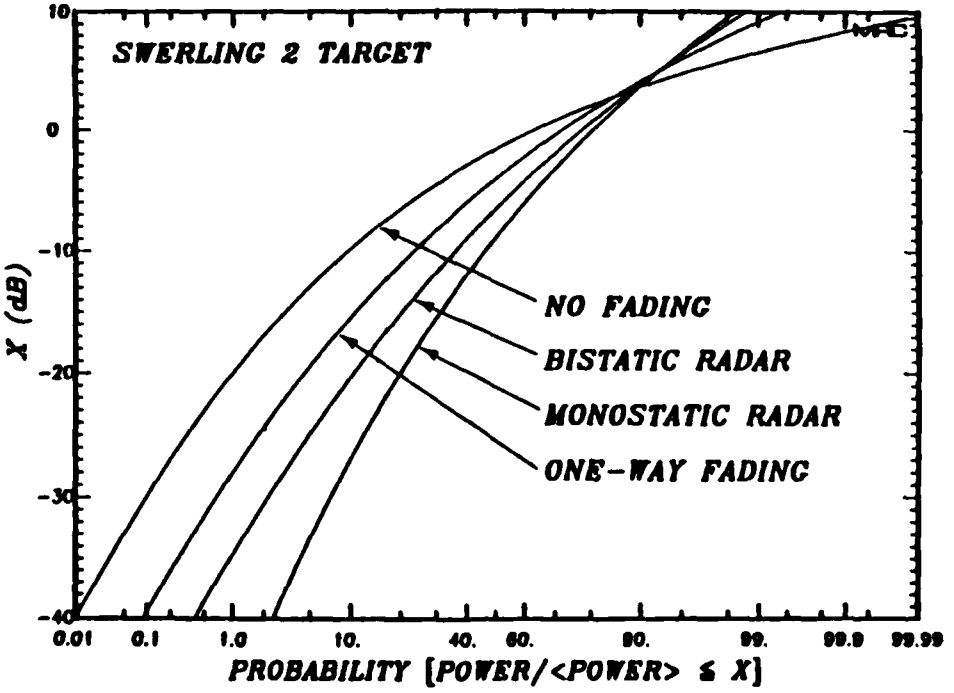

Figure 2. Cumulative probability distribution function of the received power for a Swerling 2 target and different propagation geometries.

The Swerling 2 target, with no fading, shows a probability of 10^{-4} for cross-section levels 40 dB or more below the mean value, while a monostatic radar system has a probability of two percent for the same level of fading. It has been shown (Knepp and Dana, 1982, 1983) that such fading causes degradation of SBR target detection performance.

The fading conditions described so far have assumed the worst case situation, where Rayleigh statistics characterize the one-way propagation channel. Other first-order or amplitude statistics may be used to characterize the received signal in less severely disturbed environments. However Rayleigh first-order amplitude statistics are generally associated with large spatial regions in a nuclear environment, and thus provide a useful design basis for SBR signal specification.

RECEIVED SIGNAL SECOND-ORDER STATISTICS

The second-order fading statistics are specified by the correlation function of the received complex voltage. For the case of one-way propagation of an initially constant signal through a severely disturbed ionospheric channel, the autocorrelation function of the received voltage is given as the two-position, two-frequency mutual coherence function (Knepp, 1983). For cases where the scintillation is not so severe as to cause time-delay jitter in the received waveform (i.e. pulse distortion), the single-frequency, two-position mutual coherence function is the correlation function of the signal. The effective velocity of the line-of-sight of the radar signal through the ionospheric irregularities can be utilized to convert the spatial coordinates of the mutual coherence function into

temporal coordinates, thereby obtaining the correlation function of signal fluctuations due to ionospheric irregularities. This procedure is described by Knepp (1983).

SIGNAL DECORRELATION TIME

For worst case Rayleigh fading, the correlation function of the received complex voltage E(t) always has the Gaussian form (Knepp, 1983)

$$\langle E(t)E^*(t+\tau)\rangle = \langle E(t)E^*(t)\rangle \exp(-\tau^2/\tau_0^2) \qquad (5)$$

where τ_0 is the decorrelation time (the fading rate is $1/\tau_0$) for fluctuations over the two-way propagation path from the transmitter to target and back. The actual value of τ_0 is a function of radar geometry and of the irregularity structure and intensity of the disturbed ionospheric channel. Large values of τ_0 correspond to slow fading conditions and small values to fast fading.

As a concrete example, consider the case of a radar and target separated by a layer of ionization as might occur in the case of a space based radar observing a target near the ground. For a K^{-4} in-situ power spectrum of three-dimensional ionization irregularities between outer scale L_0 and inner scale l_i, the decorrelation time is (Knepp, 1983)

$$\tau_1 = \sqrt{2}\, L_0/\ln(L_0/l_i)\sigma_\phi v_L \qquad (6)$$

where τ_1 is the decorrelation time for fluctuations over a one-way path and where

v_L = the velocity of the line-of-sight through the center of the ionized layer

$\sigma_\phi^2 = 2(r_e\lambda)^2 L_0 L \overline{\Delta N_e}^2$ rad^2

λ = RF wavelength

r_e = classical electron radius (2.82×10^{-15}m)

L = thickness of the ionized layer

$\overline{\Delta N_e}^2$ = variance of electron density irregularities.

For the monostatic SBR propagation geometry, the decorrelation time of the received signal is related to the decorrelation time for each of the one-way propagation channels according to the relationship

$$\tau_0 = \tau_1/\sqrt{2} \qquad (7)$$

where τ_1 is the decorrelation time of the one-way propagtion path.

In the work reported here it is assumed that τ_0 is large with respect to the duration of the transmitted pulse. The received signal is then coherent during the pulse duration, which is typically of the order of several tens of microseconds.

SECTION 3

RADAR SYSTEM CHARACTERISTICS

Since a space based radar must operate with relatively low transmitter power, and with targets at very long ranges, the received signal power-to-noise ratio (SNR) per pulse will be lower than that of a comparable ground based system. If, in addition, the SBR must operate in a disturbed ionospheric environment, where the signal propagation channel is subject to strong scintillation, greater demands are made on the radar system design.

A low signal-to-noise ratio implies the need for long coherent integration times, but target motion causes constructive and destructive interference from many scattering centers, resulting in rapid changes in the target cross section. To compensate, the total energy in a scan is partitioned into a number of dwells (also referred to as bursts) consisting of a number of coherent pulses which are coherently integrated upon reception. If the radar frequency is also varied sufficiently from dwell to dwell, target cross section samples will be independent, and a form of protection from jamming is provided. The detected amplitudes of all the dwells which comprise a scan are then noncoherently combined in a postdetection integration process. The resulting signal is then compared to a threshold level (which varies with the number of dwells per scan), to determine if a target has been detected during the scan.

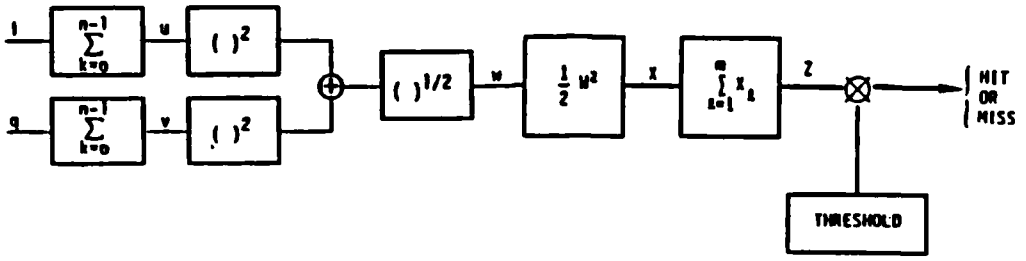

Figure 3. Block diagram of SBR receiver.

Figure 3 shows a simplified block diagram of a generic SBR receiver. The complex signal input contains amplitude, phase and doppler information from target, clutter and thermal noise sources. An appropriately weighted discrete Fourier transform (DFT) algorithm can serve both as a clutter rejection filter, and to coherently integrate the pulses in a dwell. The input to the filter can be represented by a complex valued voltage. In figure 3, the in-phase and quadrature components are denoted by i and q, respectively. The output from the filter is also a complex voltage, with components u and v. These components are coherently added, to form the amplitude w. After squaring and normalization, the output is placed in an accumulator, where the noncoherent integration takes place. Once all the dwells in a scan are received, the resulting amplitude is compared to a threshold and a "hit" or "miss" declared based upon the results of that comparison. These results are then collected in the form of probability of detection as a function of the signal-to-noise ratio, the number of dwells per scan, and the scintillation environment.

SECTION 4

PROBABILITY OF DETECTION

The major concern in this report is to determine the amount of improvement in target detection performance that would result if the SBR had knowledge of the fading rate and were able to adjust the coherent integration time. Given knowledge of the fading rate, it is assumed here that the radar processing strategy would consist in simply changing the number of dwells per scan while maintaining a constant total power on a target. The time duration of the coherent dwell (coherent integration time) would be chosen to be on the order of or greater than the signal decorrelation time in order to avoid the coherent integration loss shown in Figure 1. Although a reduction in the coherent integration time will certainly affect other aspects of radar performance (e.g. Doppler resolution, unless the pulse repetition frequency is changed), these issues are the topic of another effort.

In this report, SBR target detection performance is obtained by utilizing the MRC SBRSIM computer simulation of a space based radar.

This simulation can be operated in one of its simplest modes to repetitively collect received pulses from a Swerling 2 radar target and to combine them into a preselected number of dwells and scans as discussed in the following.

In order to assess the improvement in detection

performance, the simulation results for radar detection performance during scintillation are to be compared to the detection performance in an undisturbed propagation environment. For the case of an undisturbed propagation environment, the probability of detection may be obtained as follows.

UNDISTURBED PROPAGATION ENVIRONMENT

Under undisturbed propagation conditions, the output amplitude, z, of the noncoherent integration shown in Figure 3 has as its probability density function the expression

$$p(z) = \frac{\{z/[n\sigma_N^2(1+\langle SNR\rangle)]\}^{m-1} \exp\{-z/[n\sigma_N^2(1+\langle SNR\rangle)]\}}{n\sigma_N^2(1+\langle SNR\rangle)\Gamma(m)} \quad (8)$$

where

σ_N^2 = noise power per pulse in each complex component channel
n = the number of coherently integrated pulses
m = the number of dwells per scan
$\Gamma(m)$ = $(m-1)!$ the Gamma function
$\langle SNR\rangle$ = mean signal-to-noise ratio per dwell

The probability of detection is dependent upon the value set for the detection threshold, against which z is compared. The threshold value is, in turn, dependent upon the desired probability of false alarm. For this report the probability of false alarm, P_{fa}, is set to 10^{-6}, a typical value. The probability of false alarm is expressed as

$$P_{fa} = \int_{T}^{\infty} p(z)dz = \Gamma[m,T/(n\sigma_N^2)]/\Gamma(m) \qquad (9)$$

where $\Gamma(m,x)$ is the incomplete gamma function, and n is the number of coherently integrated pulses. Equation 9 may be numerically inverted to find T.

Once the threshold, T, has been obtained, the probability of detection is computed from

$$P_d = \int_{T}^{\infty} p(z)dz \qquad (10)$$

which is the probability that an received amplitude z of signal plus noise exceeds the detection threshold. The probability of detection may be evaluated and expressed as

$$P_d = \Gamma\{m,T/[n\sigma_N^2(1+\langle SNR\rangle)]\}/\Gamma(m) \qquad (11)$$

Equation 11 expresses the probability of detection of a Swerling 2 target as a function of the signal-to-noise ratio per dwell and of the number of dwells per scan. The probability of detection is not a function of the number of pulses per dwell as long as the received signal remains constant from pulse-to-pulse. Since this result forms the reference for SBR detection performance, it is depicted graphically in many of the following figures.

SLOW AND FAST FADING

It is useful to make a distinction between slow and fast fading that is an invaluable aid in understanding the effects of scintillation on SBR performance.

Slow fading conditions may be defined as occurring when the duration of signal fluctuations is very long compared to the coherent integration (or dwell) time. Equivalently, we say that the signal decorrelation time is much greater than the dwell time. In this case, the signal amplitude and phase are relatively constant over the dwell time, so that only dwell-to-dwell or scan-to-scan signal amplitude fluctuations affect SBR target detection performance. Examination of Equation 7 shows that, with τ representing the dwell time, and τ_0 the signal decorrelation time, the correlation function is near unity. This indicates that first order amplitude statistics are sufficient to determine the effect of slow fading on target detection performance.

Fast fading occurs when the duration of signal fluctuations is very short compared to the coherent integration (or dwell) time. We then say that the signal decorrelation time is less than the dwell time. In fast fading, many of the pulses that comprise the coherent dwell are independent. Knepp and Dana (1982) use the central limit theorem to argue that the received voltage components have independent probability distributions which may be approximated by the normal distribution.

Under slow fading conditions it is often possible to obtain

analytic expressions for the probability of detection (Knepp and Dana, 1982, 1983). However under severe fast fading conditions it is often more convenient to measure radar detection performance with the aid of simulations.

SECTION 5

RESULTS

Previous work at Mission Research Corporation (Knepp and Dana, 1982, 1983) has indicated that there is a possibility for increased radar detection performance if some of the coherent integration loss sustained under fast fading conditions can be avoided by reduction of the coherent integration time. In these results, this hypothesis is investigated over a range of fading rates and values of the number of dwells per scan. It is desirable to obtain results that will apply to a generic SBR system; because of this constraint and of the large variation in the degree of disturbance in a nuclear environment, it is useful to consider a wide range of fading rates in this work. The results presented here add to our understanding of the effects of scintillation on radar detection performance and thereby give the design engineer useful additional information.

SBRSIM

To obtain results for the probability of detection, the space based radar simulation program (SBRSIM) is used. A Swerling 2 target is utilized, and pulse trains (or dwells) are transmitted through a strongly disturbed ionized environment and then received and processed in the simulation. To simplify the calculation, perfect Doppler tracking is assumed and no clutter rejection

filtering is applied. The receiver design used in this simulation is shown in Figure 3. Here a number of coherent dwells are transmitted, each at a different radar frequency to insure that Swerling 2 target statistics apply, and to assure that the propagation environment is decorrelated between dwells. Upon reception, the pulses which comprise each dwell are integrated using a discrete Fourier transform that additionally provides for target Doppler discrimination. In this particular calculation, the target Doppler is known and no sidelobe suppression is required because the calculation is performed in the absence of clutter. The amplitude in the target range cell is then summed (noncoherently) over all the dwells which comprise a scan. This amplitude is then compared to a threshold (based on the noise power) and a hit or a miss is declared. The probability of detection is obtained simply by dividing the number of hits by the total number of scans.

To represent the fluctuating propagation channel caused by a nuclear detonation, a numerical technique known as statistical signal generation (Knepp and Wittwer, 1984) is used to generate realizations of the impulse response of the disturbed propagation channel. These signal realizations are then used by the SBRSIM code to provide the samples of the received signal for each pulse that includes the effects of scintillation. Statistical signal generation is only applicable to signal propagation through strongly ionized turbulence where the one-way signal amplitude statistics are Rayleigh.

To obtain the generic SBR detection probability results presented here, five values of the ratio τ_0/T_{SCAN} were used. These values were 0.03, 0.1, 0.2, 0.5, and 1.0. For each of these values

of τ_0/T_{SCAN}, the probability of detection was obtained for five values of the number of dwells per scan, namely 1, 2, 4, 8, and 16. For a constant value of τ_0/T_{SCAN}, then, the effect of varying the number of dwells per scan is to increase the value of the ratio of the signal decorrelation time to the coherent integration time τ_0/T_{CI} at each value of τ_0/T_{SCAN}. Therefore, from Figure 1 the coherent integration loss per dwell would decrease from what it might be otherwise. This range of values represents a wide range in the underlying values of the signal decorrelation time and should be useful for many applications involving pulse Doppler SBRs.

In general, the result of the coherent integration of a finite number of pulses is dependent upon the number of pulses. The coherent integration loss (as shown in Figure 1), is also dependent upon the number of pulses integrated. However for a large number of pulses per dwell, the coherent integration loss is independent of the number of pulses comprising the dwell. The generality of the results to be presented would be suspect unless special precautions were taken to remove the dependence upon the number of pulses per dwell. Generality is assured in the work here by increasing the number of pulses per dwell in accordance with the value of the actual decorrelation time. In many of the simulations, 128 pulses per scan are used, but for fast fading conditions and large numbers of dwells per scan, it is required that 512 pulses per scan be used to insure that the probability of detection remains independent of the number of pulses per dwell.

The need to use 512 pulses per scan to determine the coherent integration loss under fast fading conditions is also indicated by examination of Figure 1. In the figure, coherent integration loss is

shown as a function of the ratio of signal decorrelation time to coherent integration time. The curve is plotted for several values of the number of pulses that comprise the coherent dwell. The curve plotted for 16 pulses in a dwell flattens out at about 12 dB for short decorrelation times. Similarly, the curve for 32 pulses in a dwell flattens out at about 15 dB, but does so at even smaller decorrelation times. This flattening of the curve is the direct result of the use of a discrete number of pulses in a dwell. These flat areas must be avoided in this calculation in order to avoid the effect of a discrete number of pulses per dwell and to render the results more universal and, hopefully, more useful.

For example, from the figure, if the ratio of signal decorrelation time to coherent integration time is 0.04 or less, the use of only 16 pulses in a dwell would lead to a coherent integration loss of 12 dB, whereas if many pulses were used, the actual value would be larger. For a value of τ_0/T_{CI} of 0.03, 32 pulses per dwell would give adequate results. Whenever there are 16 dwells per scan, 512 pulses are required in a scan period, giving 32 pulses per dwell for this case. It is noted that the actual number of pulses per dwell used in a modern pulse Doppler radar is several hundred or more. However to obtain the results here that are independent of the number of pulses per dwell it is sufficient to use the reduced number as determined above.

Figures 4 through 8 show the major results of this study in the form of plots of the probability of detection for a Swerling 2 target as a function of the mean signal-to-noise ratio (SNR) per scan for each of the five different numbers of dwells per scan. In all cases, the probability of a false alarm is 10^{-6} as obtained through

the use of Equation 9.

Each figure contains two sets of five curves. The first set of five curves applies to the case of a Swerling 2 target with no fading, and always lies on the left hand side of the figures at the lower values of the SNR. Five curves are shown for the five values of the number of dwells per scan, 1, 2, 4, 8, and 16. This first set of curves is identical in each of the five figures, and is provided to serve as a reference for the results pertaining to severe scintillation.

The other set of five curves in each of the figures was obtained for the case of severe fading for the same five values of the number of dwells per scan, that is 1, 2, 4, 8, and 16. In each of the five figures the ratio τ_0/T_{SCAN} takes on a different value. The ratio τ_0/T_{SCAN} has the values 0.03, 0.1, 0.2, 0.5, and 1.0 in Figures 4-8, respectively. These figures present a wide range of fading rates for a space based radar. In Figure 4 where the results for the fastest fading are presented for a value of τ_0/T_{SCAN} of 0.03, it can be seen that the two sets of five curves fall far apart, indicating a large loss in detection performance in fast fading, even after an increase in the number of dwells per scan. However it is apparent from Figure 4 that an increase in the number of dwells per scan gives improved performance. In Figure 8, for the slowest fading considered here where τ_0/T_{SCAN} is equal to 1.0, it is seen that an increase in the number of dwells per scan can greatly improve the radar detection performance. The measured probabilities of detection in Figures 4-13 have an average error of 0.05, associated with the finite number of measurements.

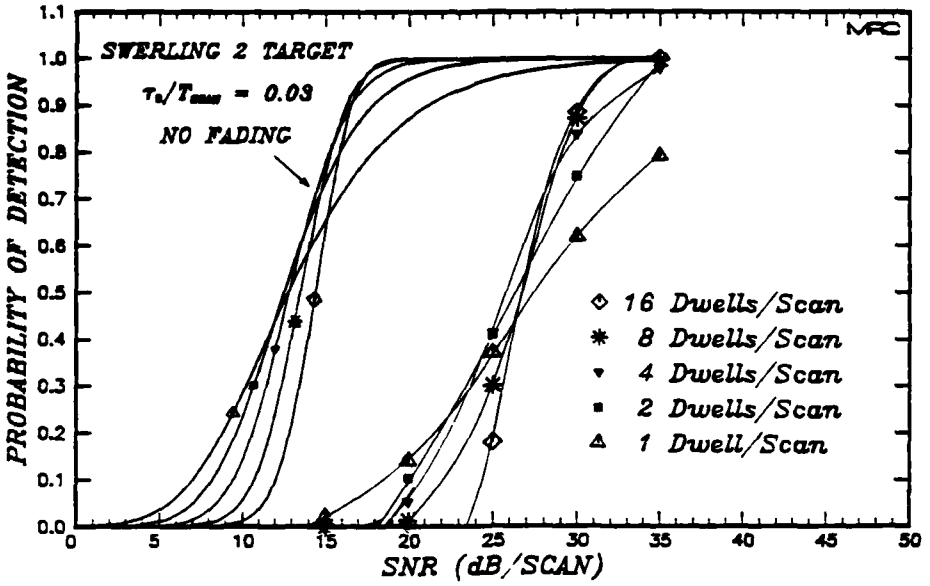

Figure 4. Probability of detection vs mean signal-to-noise ratio as a function of the number of dwells per scan, τ_0/T_{SCAN} = 0.03.

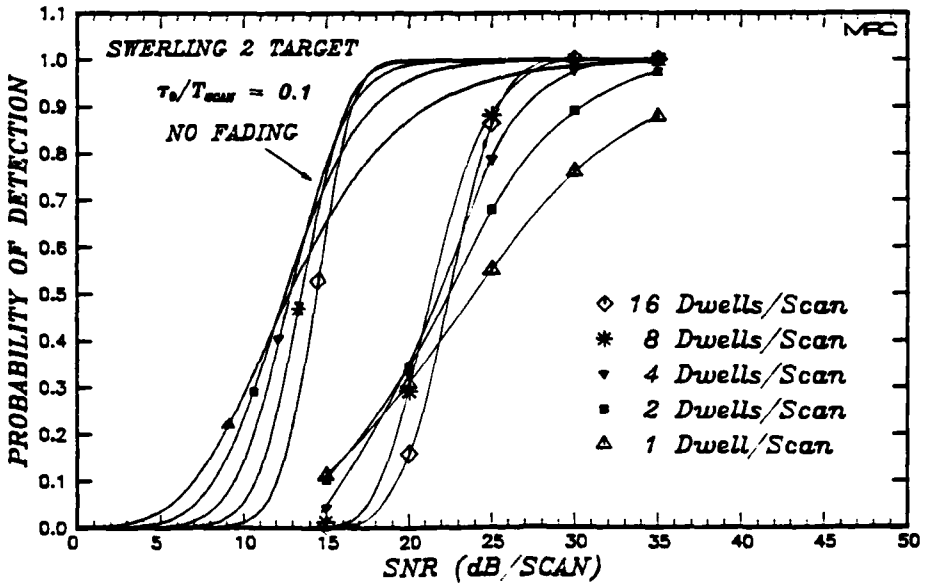

Figure 5. Probability of detection vs mean signal-to-noise ratio as a function of the number of dwells per scan, τ_0/T_{SCAN} = 0.1.

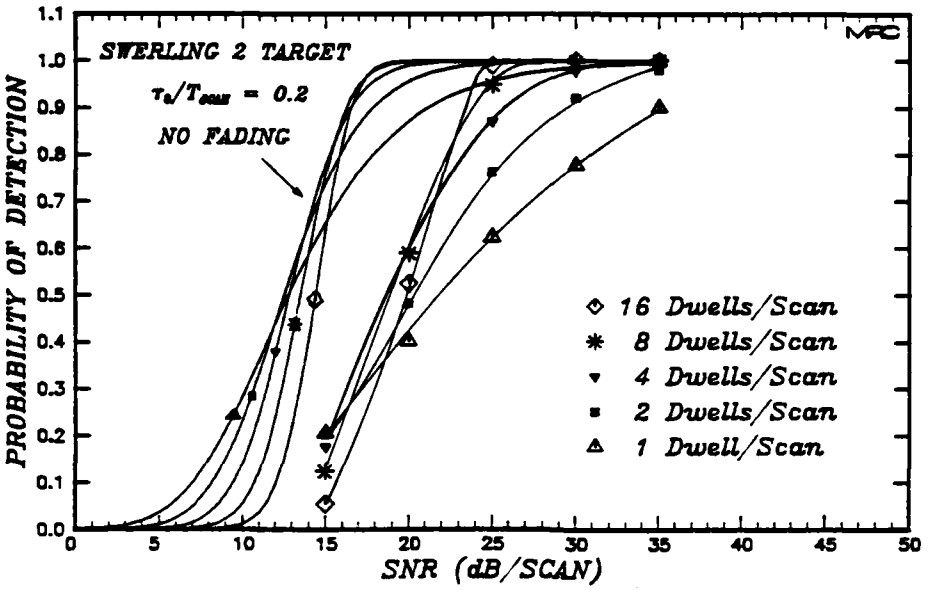

Figure 6. Probability of detection vs mean signal-to-noise ratio as a function of the number of dwells per scan, τ_0/T_{SCAN} = 0.2.

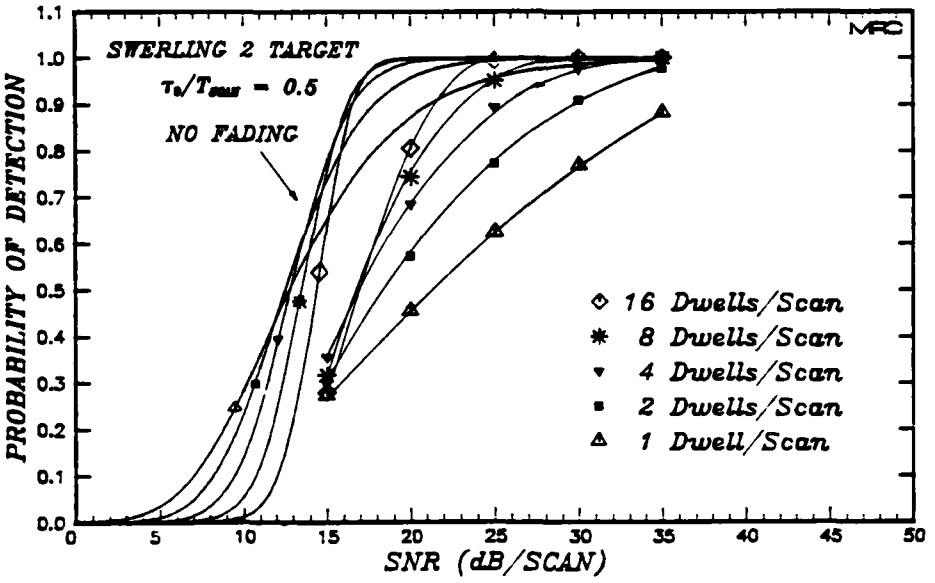

Figure 7. Probability of detection vs mean signal-to-noise ratio as a function of the number of dwells per scan, τ_0/T_{SCAN} = 0.5.

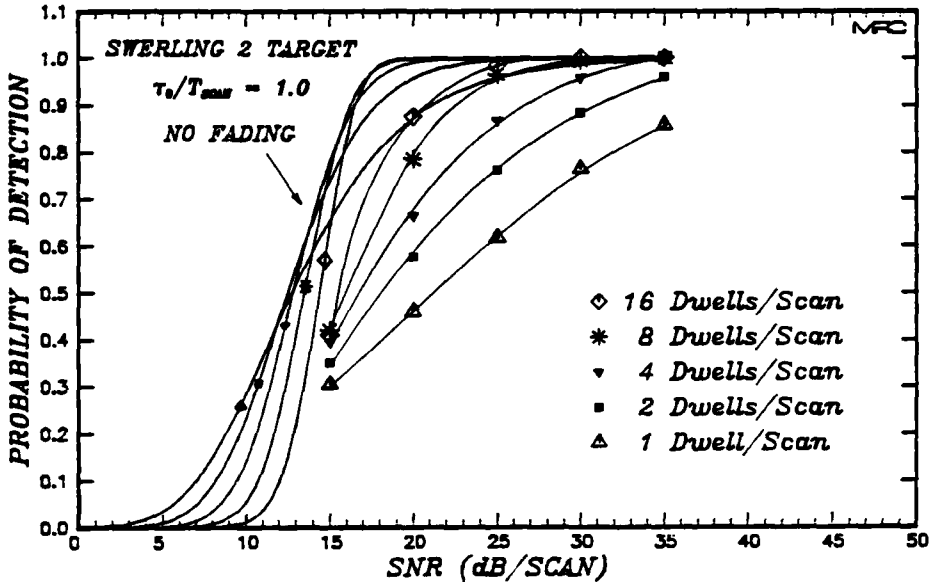

Figure 8. Probability of detection vs mean signal-to-noise ratio as a function of the number of dwells per scan, τ_0/T_{SCAN} = 1.0.

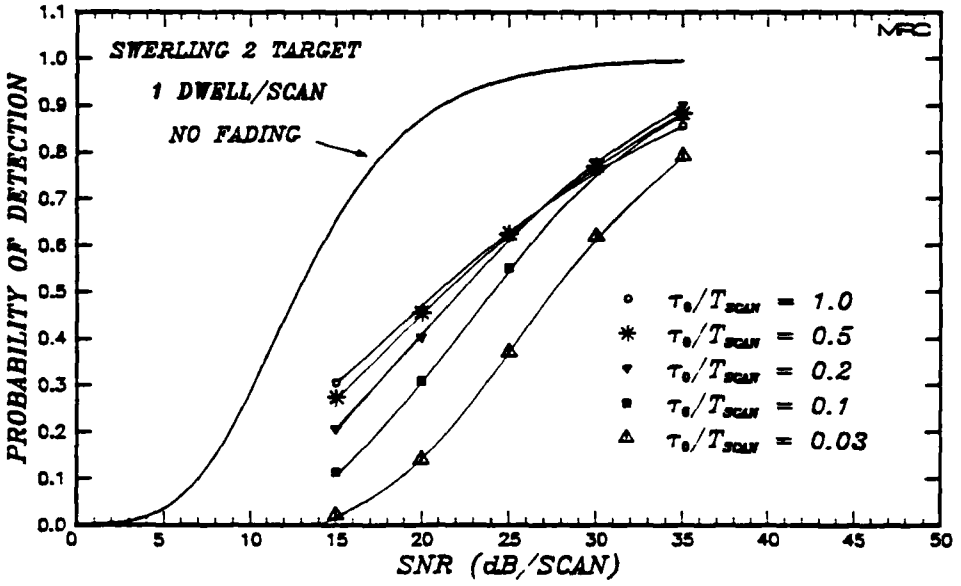

Figure 9. Probability of detection vs mean signal-to-noise ratio as a function of τ_0/T_{SCAN} for 1 dwell per scan.

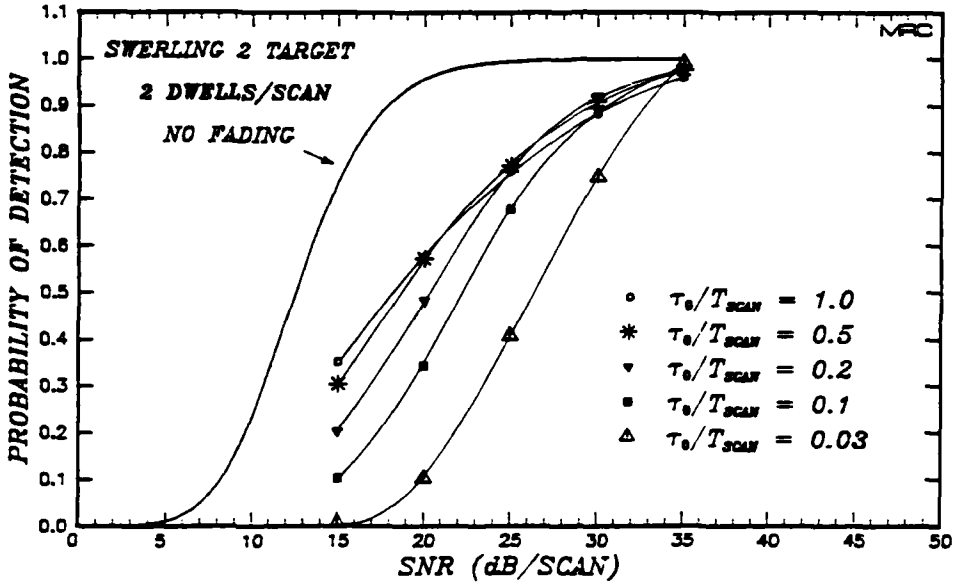

Figure 10. Probability of detection vs mean signal-to-noise ratio as a function of τ_0/T_{SCAN} for 2 dwells per scan.

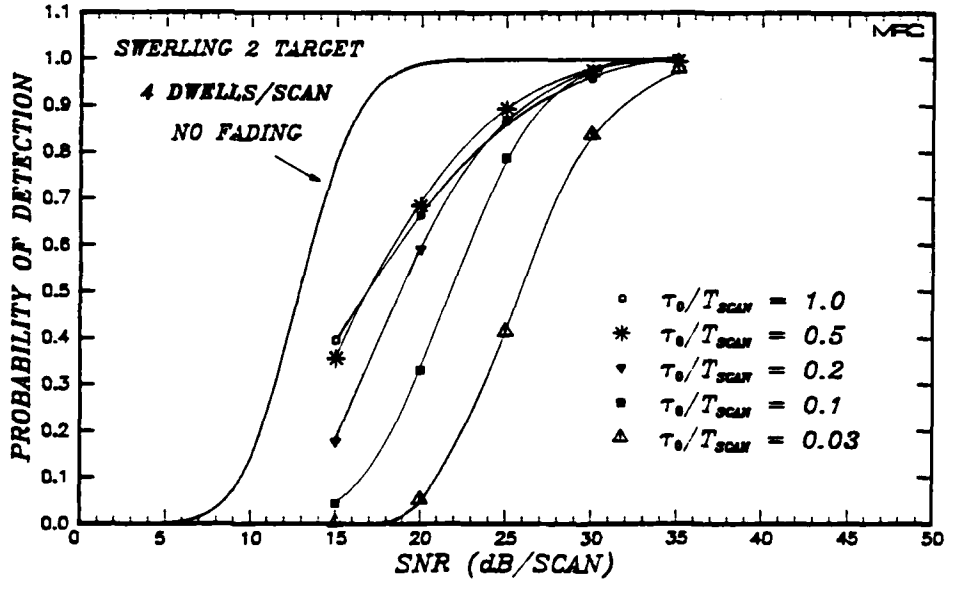

Figure 11. Probability of detection vs mean signal-to-noise ratio as a function of τ_0/T_{SCAN} for 4 dwells per scan.

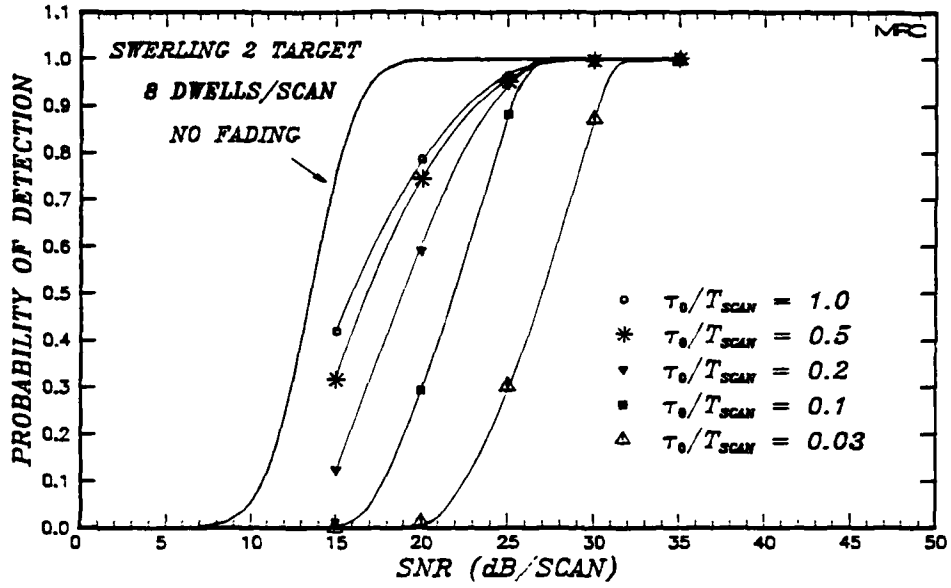

Figure 12. Probability of detection vs mean signal-to-noise ratio as a function of τ_0/T_{SCAN} for 8 dwells per scan.

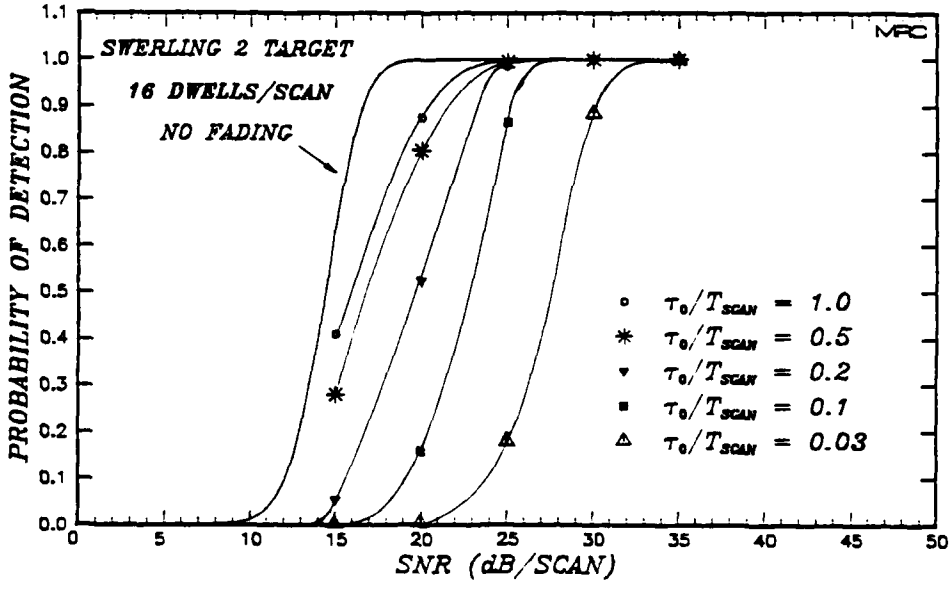

Figure 13. Probability of detection vs mean signal-to-noise ratio as a function of τ_0/T_{SCAN} for 16 dwells per scan.

Figures 9-13 present the same results, but in a different format where each figure depicts the probability of detection for a fixed value of the number of dwells per scan. One value of this format is that it gives the radar designer measurements of the performance of a system with a fixed number of dwells per scan as a function of the fading rate or τ_0. The appropriate curve for an undisturbed propagation environment is also shown in each figure.

It is immediately obvious that, if the fading rate increases (τ_0 decreases), the SNR required to obtain a given probability of detection increases. By varying the number of dwells per scan, the SBR designer can offset this somewhat. That is, by an appropriate choice of the number of dwells per scan, the SNR required to achieve a given probability of detection can be minimized.

THE OPTIMAL NUMBER OF DWELLS PER SCAN

One method to determine the optimum number of dwells per scan is described in Knepp and Dana (1983). The optimum number of dwells per scan may be determined by finding that detection curve which, for probabilities of detection above 0.5, minimizes the difference between the SNR required to achieve a given probability of detection, and the minimum SNR required to achieve that same probability of detection. For an undisturbed propagation environment, the optimum number of dwells per scan is four. In part, this choice is predicated on another criterion, which requires that the detection performance degrade gracefully until the probability of detection falls below the minimum value required to maintain a radar track. This minimum value is assumed to be 0.5 in this work.

Essentially, this is a requirement on the sensitivity of the probability of detection to changes in the signal-to-noise ratio. This same criterion for choosing the optimum number of dwells per scan may be used for design purposes in a fading environment.

It is clear from an examination of the figures that the SNR minimization process described above does not necessarily result in the choice of a detection curve that gives the smallest decrease in probability of detection with decreasing signal-to-noise ratio. Although we do not take this effect into account in choosing the optimal number of dwells per scan, an SBR designer with specific design requirements may have a need to do so.

In order to choose the optimal detection curve for each of the five values of τ_0/T_{SCAN} the following graphical procedure was adopted. For each value of τ_0/T_{SCAN} in each of the five figures numbered from 4-8, values of probability of detection of 0.5, 0.6, 0.7, 0.8, and 0.9 were examined. Then for each of the five different values of number of dwells per scan, the difference (in decibels) in SNR between the individual curves and the best curve was determined. These differences are presented in Tables 1-5 for each of the five values of τ_0/T_{SCAN}, respectively. Only values of 4, 8 and 16 dwells per scan are presented here since these curves were always superior to those corresponding to 1 and 2 dwells per scan. The table then consists of values of the deviation of the SNR from the optimum value measured at five different values of the probability of detection. The optimum number of dwells per scan is chosen for which the mean deviation (averaged in decibels over the five values of probability of detection shown in the table) from the best value is least. Tables 1 through 5 show the deviations for the five values of

τ_0/T_{SCAN}, as well as their mean. An asterisk at the end of a line corresponding to a fixed number of dwells per scan in Table 1-5 shows the value of the number of dwells per scan that is chosen as optimum. Note that in Table 1, for τ_0/T_{SCAN} equal to 0.03, the difference in the means was not great enough to warrant choosing between 4, 8 or 16 dwells per scan.

Table 6 summarizes the results for the optimum number of dwells per scan at each of the values of τ_0/T_{SCAN} and probability of detection. The overall optimum choice for the number of dwells per scan based on the average SNR deviation from optimum at each probability of detection is also included as the final column in Table 6. It is evident from Table 6 that minimization of SNR requirements during fading requires dynamic variation of the number of dwells per scan.

Note that the rule for the choice of the best number of dwells per scan was made for probabilities of detection between 0.5 and 0.9. Another choice of probabilities of detection might yield somewhat different results. Also, weighting the choices of probability of detection might result in a different set of choices.

Table 1. Difference of SNR (dB) measured versus the minimum SNR at that probability of detection for 4, 8, and 16 dwells per scan when $\tau_0/T_{SCAN} = 0.03$.

Dwells Per Scan	Probability of Detection 0.5	0.6	0.7	0.8	0.9	mean
4	0.0	0.0	0.0	0.4	1.6	0.4 *
8	1.0	0.7	0.2	0.1	0.0	0.4 *
16	1.0	0.5	0.0	0.0	0.0	0.3 *

Table 2. Difference of SNR (dB) measured versus the minimum SNR at that probability of detection for 4, 8, and 16 dwells per scan when $\tau_0/T_{SCAN} = 0.1$.

Dwells Per Scan	Probability of Detection 0.5	0.6	0.7	0.8	0.9	mean
4	0.5	1.0	1.1	1.4	1.7	1.1
8	0.0	0.0	0.0	0.0	0.0	0.0 *
16	1.1	1.0	0.8	0.7	0.2	0.8

Table 3. Difference of SNR (dB) measured versus the minimum SNR at that probability of detection for 4, 8, and 16 dwells per scan when $\tau_0/T_{SCAN} = 0.2$.

Dwells Per Scan	Probability of Detection 0.5	0.6	0.7	0.8	0.9	mean
4	0.0	0.0	0.5	1.1	2.3	0.8
8	0.2	0.0	0.0	0.0	0.4	0.1 *
16	1.1	0.7	0.4	0.2	0.0	0.5

Table 4. Difference of SNR (dB) measured versus the minimum SNR at that probability of detection for 4, 8, and 16 dwells per scan when $\tau_0/T_{SCAN} = 0.5$.

Dwells Per Scan	Probability of Detection 0.5	0.6	0.7	0.8	0.9	mean
4	0.2	0.5	1.4	2.7	4.1	1.8
8	0.0	0.0	0.3	0.9	1.6	0.6
16	0.2	0.0	0.0	0.0	0.0	0.04 *

Table 5. Difference of SNR (dB) measured versus the minimum SNR at that probability of detection for 4, 8, and 16 dwells per scan when $\tau_0/T_{SCAN} = 1.0$.

Dwells Per Scan	Probability of Detection 0.5	0.6	0.7	0.8	0.9	mean
4	1.3	2.3	3.2	5.5	5.8	3.6
8	0.4	1.2	1.3	1.5	1.7	1.2
16	0.0	0.0	0.0	0.0	0.0	0.0 *

Table 6. The number of dwells per scan which give the minimum SNR.

τ_0/T_{SCAN}	Probability of Detection 0.5	0.6	0.7	0.8	0.9	Best choice
0.03	4	4	4/16	16	8/16	4/8/16
0.1	8	8	8	8	8	8
0.2	4	4/8	8	8	8	8
0.5	8	8/16	16	16	16	16
1.0	16	16	16	16	16	16

Table 7. Improvement in SNR (dB) between the minimum SNR at a given probability of detection and the SNR for 4 dwells per scan.

τ_0/T_{SCAN}	Probability of Detection 0.5	0.6	0.7	0.8	0.9
0.03	0.0	0.0	0.0	0.4	1.6
0.1	0.5	1.0	1.1	1.4	1.7
0.2	0.0	0.0	0.5	1.1	2.3
0.5	0.2	0.5	1.4	2.7	4.1
1.0	1.3	2.3	3.3	5.5	5.8

Recall that the optimum number of dwells per scan in an ambient, unperturbed propagation environment was found to be 4 (Knepp and Dana, 1983). For that reason, it is useful to measure any performance increases (decreases in SNR) relative to the SNR that would be required if the dwells per scan were held constant at 4. Table 7 summarizes this information. The results in this table can be obtained from Tables 1-5 by comparing the values for 8 and 16 dwells per scan with those for 4 dwells per scan. In most table entries, the SNR required at 4 dwells per scan is greater than that required using the optimum choice which is usually 8 or 16 dwells per scan. If the SNR required at 4 dwells per scan is smaller than that required for the optimum choice, then a zero is entered in the table.

In Figure 14, the "improvement factor" of Table 7, measured in dB, is plotted as a function of the ratio of signal decorrelation time to scan time, for 3 different values of probability of detection. The data for these curves was obtained by visual examination of Figures 4-8, and is not exact. The presence of the bump at 0.1 on the abscissa is probably due to a combination of measurement error, and the fact that the curves in Figures 4-8 tend to intersect at different points in each figure.

It is apparent from Figure 14 that it is possible to obtain an improvement in the detection performance of the system by varying the number of dwells per scan. This increase in performance can be as much as 6 dB, for probabilities of detection of about 0.9. At a more modest probability of detection of 0.7, an increase in performance of nearly 3 dB is attainable.

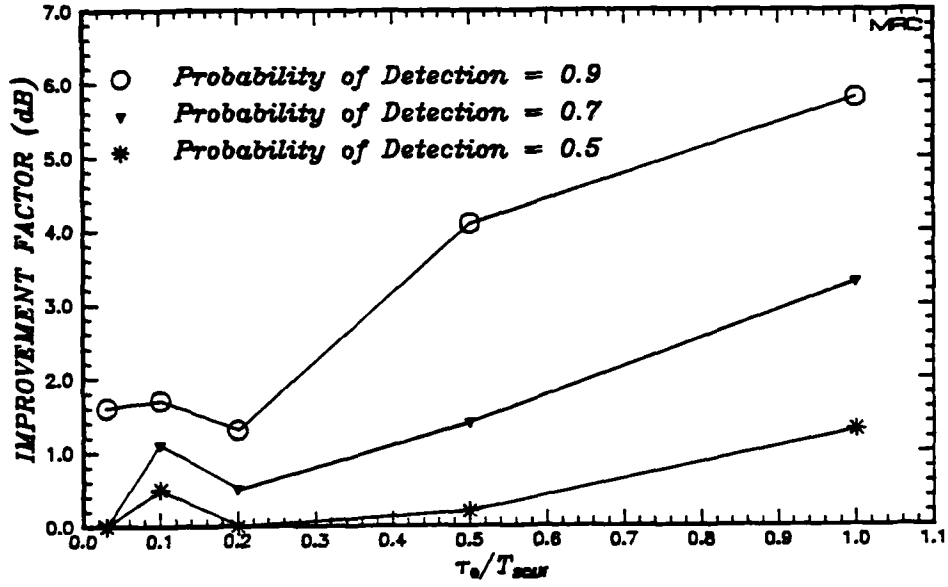

Figure 14. Improvement factor vs τ_0/T_{SCAN} for 3 values of probability of detection.

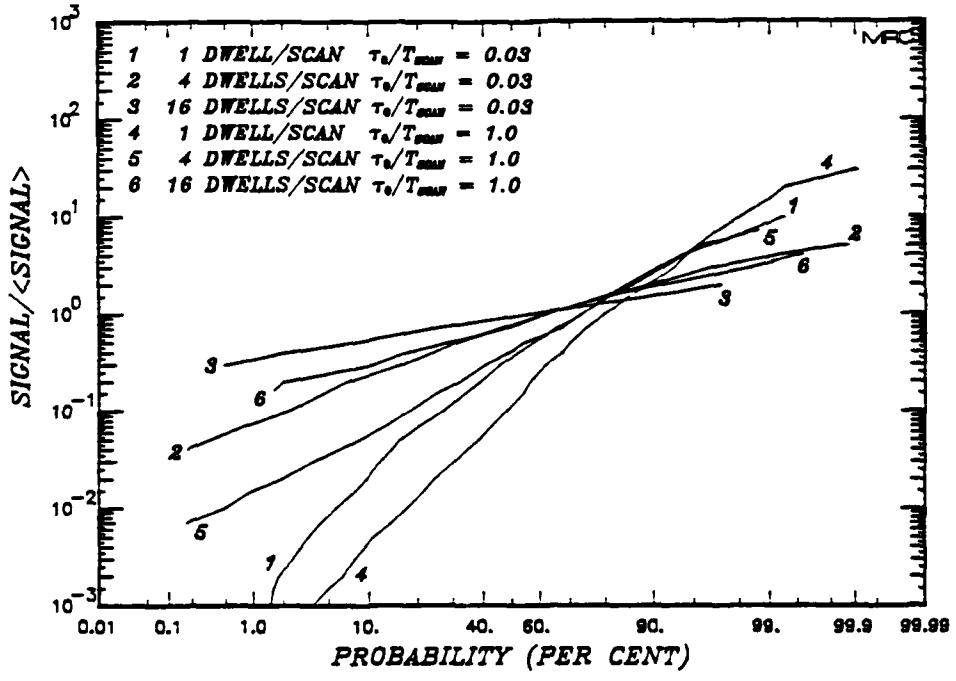

Figure 15. Cumulative probability distribution of output power for various τ_0/T_{SCAN} and numbers of dwells per scan.

THE INFLUENCE OF STATISTICS

It is useful to examine the shape of the curves in Figures 4-8, and consequently of Figure 14 in order to understand the reasons for the improvements obtained. It is evident from this study that increasing the number of dwells per scan is more effective in slow fading than in fast fading. The differences in the shape of the detection curves for different numbers of dwells per scan at slow fading seem to indicate that the probability distributions change with the number of dwells per scan. To check this hypothesis, the SBRSIM simulation was temporarily modified to yield the probability distributions of the received signal power. Figure 15 shows some of the results, in the form of cumulative probability distribution functions.

Figure 15 shows the cumulative probability distributions of the power at the output of the noncoherent integrator. The abscissa shows the value of the received signal power divided by the mean power. To obtain these results for the cumulative power distributions of the signal alone, the simulation was utilized in a zero noise condition. Two values of τ_0/T_{SCAN} are shown in the figure, 0.03 and 1.0 respectively. These represent the slowest and fastest fading rates considered in this study. For each of these values of τ_0/T_{SCAN}, the number of dwells per scan are taken as 1, 4 and 16. The two curves labeled 2 and 3 in the figure for a value of τ_0/T_{SCAN} of 0.03 are seen to fall close together, indicating that there is very little change in the statistics at the output of the noncoherent integrator for this value of τ_0/T_{SCAN} for values of 4 to 16 dwells per scan. This result is simply a verification of results presented previously that show little change in probability of

detection as the number of dwells is increased. The other three curves labeled 4, 5 and 6 for slow fading conditions where τ_0/T_{SCAN} is 1.0 show a change toward a probability distribution with less variation as the number of dwells per scan is increased. A horizontal line on this figure at an abscissa value of unity would indicate a constant signal, and variation in the signal is seen as cumulative distribution curves with larger slopes.

An interesting feature in this figure is that the curve representing 16 dwells per scan at slow fading (τ_0/T_{SCAN} = 1.0) is nearly the same as the curve for 4 dwells per scan at fast fading (τ_0/T_{SCAN} = 0.03). This implies that under fast fading conditions, the noncoherent summation of the power from many dwells does not affect the output signal statistics much. This is evident because of the similarity of curves 2 and 3 in Figure 15. Thus in fast fading conditions, since the output power variation is small, a decrease in the signal threshold may be effective in yielding increased detection performance, of course with a greater false alarm probability. In slow fading, the noncoherent integration of the power from multiple dwells improves detection performance because it reduces the variability of the output power. By an analogy with laser speckle processes (Goodman, 1976), we may say that increasing the number of independent samples decreases the contrast, allowing the desired signal to be perceived more easily.

SECTION 6

CONCLUSIONS

A space based radar system may be confronted with operating environments in which the signal propagation paths are severely disturbed, resulting in rapid scintillation of the received signal and diminished radar detection and tracking performance. Part of the ongoing mitigation effort to design a system that can optimize performance in such an environment has focussed on the use of noncoherent integration of multiple coherent dwells in a scan. This report investigates the possiblity that if knowledge of the fading rate were available, a space based radar could improve target detection performance by utilizing an adaptive processing strategy.

Previous work (Knepp and Dana, 1983) indicated that there is a possibility of deriving some gain in target detection performance by changing the number of coherent dwells in a scan under severe fading conditions. This report has investigated this hypothesis and has quantified the conditions under which such a gain is possible and has presented calculations for the gain.

The original hypothesis has been confirmed, and the following results discovered. By dynamically changing the number of dwells per scan as a function of the fading environment, it is possible to reduce the required SNR to achieve a probability of detection of 0.9 by as much as 6 dB, during slow fading. During fast fading, gains are more modest, especially during fast fading where the signal decorrelation time is less than about one-tenth of the

scan time, when gains are generally less than 1 dB.

Note that this report has considered only the effect on radar detection performance of specific changes in radar design. Therefore other important radar design issues that would be affected by design changes investigated here have been ignored. Before an SBR design is completed these other issues must be addressed. For example, this work has not considered the possible decrease in clutter rejection performance and Doppler resolution that would occur if the coherent integration time or dwell duration were to be reduced. The mitigation techniques investigated here require further investigation in the context of a complete SBR system.

SECTION 7

LIST OF REFERENCES

Arendt, P. R., and H. Soicher, "Effects of Arctic Nuclear Explosions on Satellite Radio Communication," Proc. IEEE, Vol. 52, No. 6, pp. 672-676, June 1964.

Davis, T. N., G. J. Romick, E. M. Westcott, R. A. Jeffries, D. M. Kerr, and H. M. Peek, "Observations of the Development of Striations in Large Barium Clouds," Planet. Space Science, Vol. 22, p. 67, 1974.

Fante, R. L., "Electromagnetic Beam Propagation in Turbulent Media," Proc. IEEE, Vol. 63, No. 12, pp. 1669-1692, December 1975.

Fremouw, E. J., R. L. Leadabrand, R. C. Livingston, M. D. Cousins, C. L. Rino, B. C. Fair and R. A. Long, "Early Results from the DNA Wideband Satellite Experiment-Complex Signal Scintillation," Radio Science, Vol. 13, No. 1, pp. 167-187, January-February 1978.

Goodman, J. W., "Some Fundamental Properties of Speckle," J. Opt. Soc. Am., Vol. 66, pp. 1145-1150, 1976.

King, M. A., and P. B. Fleming, "An Overview of the Effects of Nuclear Weapons on Communications Capabilities," Signal, pp. 59-66, January 1980.

Knepp, D. L., Multiple Phase-Screen Propagation Analysis for Defense Satellite Communications System, DNA 4424T, MRC-R-332, Mission Research Corporation, September 1977.

Knepp, D. L., and R. A. Dana, "Impact of the Propagation Environment on Space Based Radar Design," AIAA-82-0424, AIAA 20th Aerospace Sciences Meeting, Orlando, Florida, January 1982.

Knepp, D. L., "Analytic Solution for the Two-Frequency Mutual Coherence Function for Spherical Wave Propagation," Radio Science, Vol. 18, No. 4, pp. 535-549, July-August 1983.

Knepp, D. L., and R. A. Dana, The Impact of Strong Scintillation on Space Based Radar Design -- Noncoherent Detection, DNA-TR-83-43, MRC-R-788, Mission Research Corporation, November 1983.

Knepp, D. L., and L. A. Wittwer, "Simulation of Wide Bandwidth Signals That Have Propagated Through Random Media," Radio Science, Vol. 19, No. 1, pp. 303-308, January-February 1984.

Pope, J. H., and R. B. Fritz, "High Latitude Scintillation Effects on Very High Frequency (VHF) and S-band Satellite Transmissions," Indian J. Pure App. Phys., Vol. 9, pp. 593-600, August 1971.

Skinner, N. J., R. F. Kelleher, J. B. Hacking and C. W. Benson, "Scintillation Fading of Signals in the SHF Band," Nature (Phys. Sci.), Vol. 232, pp. 19-21, 5 July 1971.

Taur, R. R., "Simultaneous 1.5- and 4-GHz Ionospheric Scintillation Measurements," Radio Science, Vol. 11, pp. 1029-1036, December 1976.

Wittwer, L. A., A Trans-Ionospheric Signal Specification for Satellite C^3 Applications, DNA 5662D, Defense Nuclear Agency,

December, 1980.

Wolcott, J. H., D. J. Simons, T. E. Eastman, and T. J. Fitzgerald, "Characteristics of Late-Time Striations Observed During Operation STRESS," Effect of the Ionosphere on Space and Terrestrial Systems, edited by J. M. Goodman, pp. 602-613, U.S. Government Printing Office, 1978.

DISTRIBUTION LIST

DEPARTMENT OF DEFENSE

Assist Secy of Def, Comd, Cont, Comm & Intel
ATTN: DADSD(I)
ATTN: Dir of Intelligence Sys

Command & Control Sys Org
ATTN: G500, R. Crawford
ATTN: G510, G. Jones
ATTN: G510, P. Bird

Defense Advanced Rsch Proj Agency
ATTN: GSD, R. Alewine
ATTN: T. Iether

Defense Communications Agency
ATTN: Code 230
ATTN: J300 for Yen-Sun Fu

Defense Communications Engineer Ctr
ATTN: Code R123, Tech Lib
ATTN: Code R410, N. Jones

Defense Intelligence Agency
ATTN: DB, A. Wise
ATTN: DB-4C
ATTN: DC-7B
ATTN: Dir
ATTN: DT-1B
ATTN: RTS-2B

Defense Nuclear Agency
ATTN: NATF
ATTN: NAWE
ATTN: RAAE, P. Lunn
ATTN: RAEE
ATTN: STNA
3 cys ATTN: RAAE
4 cys ATTN: STTI-CA

Defense Technical Information Center
12 cys ATTN: DD

Field Command, DNA, Det 2
Lawrence Livermore National Lab
ATTN: FC-1

Field Command, Defense Nuclear Agency
ATTN: FCPR
ATTN: FCTT, W. Summa
ATTN: FCTXE

Interservice Nuclear Weapons School
ATTN: TTV

Joint Chiefs of Staff
ATTN: C3S
ATTN: C3S, Evaluation Office (HDOO)

Joint Data System Support Ctr
ATTN: C-312, R. Mason

Joint Strat Tgt Planning Staff
ATTN: JLK, DNA Rep
ATTN: JLKS
ATTN: JPPFD
ATTN: JPSS
ATTN: JPTM

DEPARTMENT OF DEFENSE (Continued)

National Security Agency
ATTN: B-43, C. Goedeke

Under Secy of Def for Rsch & Engrg
ATTN: Strat & Space Sys (OS)

DEPARTMENT OF THE ARMY

Army Logistics Management Ctr
ATTN: DLSIE

Assist Ch of Staff for Automation & Comm
ATTN: DAMO-C4, P. Kenny

Atmospheric Sciences Lab
US Army Electronics R & D Command
ATTN: DELAS-EO, F. Niles

BMD Advanced Technology Center
ATTN: ATC-R, D. Russ
ATTN: ATC-R, W. Dickinson

BMD Systems Command
ATTN: BMDSC-LEH, R. Webb
2 cys ATTN: BMDSC-HW

Dep Ch of Staff for Ops & Plans
ATTN: DAMO-RQC, C2 Div

Harry Diamond Laboratories
ATTN: DELHD-NW-R, R. Williams
ATTN: SLCHD-NW-P

US Army Chemical School
ATTN: ATZN-CM-CS

US Army Comm-Elec Engrg Instal Agency
ATTN: CC-CE-TP, W. Nair

US Army Communications R&D Command
ATTN: DRDCO-COM-RY, W. Kesselman

US Army Foreign Science & Tech Ctr
ATTN: DRXST-SD

US Army Information Systems Cmd
ATTN: CC-OPS-W
ATTN: CC-OPS-WR, H. Wilson

US Army Material Command
ATTN: DRCLDC, J. Bender

US Army Nuclear & Chemical Agency
ATTN: Library

US Army Satellite Comm Agency
ATTN: Document Control

US Army TRADOC Sys Analysis Actvy
ATTN: ATAA-PL
ATTN: ATAA-TCC, F. Payan, Jr.
ATTN: ATAA-TDC

DEPARTMENT OF THE NAVY

Joint Cruise Missiles Project Ofc (PM-23)
ATTN: JCMG-707

DEPARTMENT OF THE NAVY (Continued)

Naval Air Systems Command
ATTN: PMA-271

Naval Intelligence Support Ctr
ATTN: NISC-50

Naval Research Laboratory
ATTN: Code 4108, P. Rodriguez
ATTN: Code 4187
ATTN: Code 4700
ATTN: Code 4720, J. Davis
ATTN: Code 4780
ATTN: Code 6700
ATTN: Code 7500, B. Wald
ATTN: Code 7950, J. Goodman

Naval Space Surveillance System
ATTN: J. Burton

Naval Surface Weapon Ctr, White Oak Lab
ATTN: Code F31

Naval Telecommunications Command
ATTN: Code 341

Ofc of the Dep Chief of Naval Ops
ATTN: NOP 654, Strat Eval & Anal Br
ATTN: NOP 981N
ATTN: NOP 941D

Office of Naval Research
ATTN: Code 412, W. Condell

Space and Naval Warfare Systems Cmd
ATTN: Code 3101, T. Hughes
ATTN: Code 501A
ATTN: PDE-110-X1, B. Kruger
ATTN: PDE-110-11021, G. Brunhart
ATTN: PME 106-4, S. Kearney
ATTN: PME 117-20
ATTN: PME-106, F. Diederich

Strategic Systems Programs (PM-1)
ATTN: NSP-2141
ATTN: NSP-2722
ATTN: NSP-43, Tech Lib

Naval Sea Systems Command
ATTN: PMS-423, D. Smith

DEPARTMENT OF THE AIR FORCE

Air Force Geophysics Laboratory
ATTN: CA, A. Stair
ATTN: LID, J. Ramussen
ATTN: LIS, J. Buchau
ATTN: LYD, K. Champion
ATTN: OPR-1
ATTN: R. Babcock
ATTN: R. O'Neil

Air Force Satellite Ctrl Facility
ATTN: WE

Air Force Space Technology Ctr
ATTN: YH

Air Force Weapons Laboratory
ATTN: NTN
ATTN: SUL

DEPARTMENT OF THE AIR FORCE (Continued)

Air Force Wright Aeronautical Lab/AAAD
ATTN: A. Johnson
ATTN: W. Hunt

Air Logistics Command
ATTN: OO-ALC/MM

Air University Library
ATTN: AUL-LSE

Assist Ch of Staff, Studies & Analysis
ATTN: AF/SASC, C. Rightmeyer

Ballistic Missile Office/DAA
ATTN: ENSN
ATTN: ENSN, W. Wilson
ATTN: SYC, D. Kwan

Dep Chief of Staff, Rsch, Dev, & Acq
ATTN: AF/RDQI
ATTN: AFRDS, Space Sys & C3 Dir

Electronic Systems Division
ATTN: SCS-1E
ATTN: SCS-2, G. Vinkels

Foreign Technology Division
ATTN: NIIS, Library
ATTN: TQTD, B. Ballard

Rome Air Development Center
ATTN: OCS, V. Coyne
ATTN: OCSA, R. Schneible
ATTN: TSLD

Rome Air Development Center
ATTN: EEPS, P. Kossey

Space Command
ATTN: DC, T. Long

Strategic Air Command
ATTN: SAC/LGW
ATTN: NRI/STINFO
ATTN: XPFC
ATTN: XPFS
ATTN: XPQ

DEPARTMENT OF ENERGY

Department of Energy, GTN
ATTN: DP-233

EG&G, Inc
ATTN: D. Wright
ATTN: J. Colvin

University of California
Lawrence Livermore National Lab
ATTN: L-658, Tech Info Dept Library

Los Alamos National Laboratory
ATTN: D. Sappenfield
ATTN: G-6, E. Jones

Sandia National Laboratories
ATTN: D. Hartley, 8300
ATTN: T. Cook

DEPARTMENT OF ENERGY (Continued)

Sandia National Laboratories
ATTN: D. Dahlgren
ATTN: D. Thornbrough
ATTN: Org 1231, R. Backstrom
ATTN: Org 1250, W. Brown
ATTN: Space Project Div
ATTN: Tech Lib, 3141

OTHER GOVERNMENT AGENCIES

US Dept of State, Bureau of Politico Mil Affairs
ATTN: PM/STM

Central Intelligence Agency
ATTN: OSWR/SSD for K. Feuerpfetl

Dept of Commerce, National Bureau of Standards
ATTN: Sec Ofc for R. Moore

Dept of Commerce, National Oceanic & Atmos Admin
ATTN: R. Grubb

US Dept of Commerce, NOAA/MASC Security Ofc
ATTN: A. Jean
ATTN: W. Utlaut

DEPARTMENT OF DEFENSE CONTRACTORS

Aerospace Corp
ATTN: D. Olsen
ATTN: D. Whelan
ATTN: I. Garfunkel
ATTN: J. Kluck
ATTN: J. Straus
ATTN: K. Cho
ATTN: R. Slaughter
ATTN: T. Salmi
ATTN: V. Josephson

Aerospace Corp
ATTN: S. Mewaters

Analytical Systems Engineering Corp
ATTN: Radio Sciences

Analytical Systems Engineering Corp
ATTN: Security

Austin Research Associates
ATTN: J. Thompson

Autometric, Inc
ATTN: C. Lucas

BDM Corp
ATTN: L. Jacobs
ATTN: T. Neighbors

Berkeley Rsch Associates, Inc
ATTN: J. Workman
ATTN: S. Brecht

Boeing Co
ATTN: G. Hall

Boeing Co
ATTN: MS 8K-85, Dr. S. Tashird

BR Communications
ATTN: J. McLaughlin

DEPARTMENT OF DEFENSE CONTRACTORS (Continued)

California Research & Technology, Inc
ATTN: M. Rosenblatt

University of California at San Diego
ATTN: H. Booker

Charles Stark Draper Lab, Inc
ATTN: A. Tetewski
ATTN: D. Cox
ATTN: J. Gilmore

Communications Satellite Corp
ATTN: G. Hyde

Computer Sciences Corp
ATTN: F. Eisenbarth

Cornell University
ATTN: D. Farley, Jr.
ATTN: M. Kelly

Electrospace Systems, Inc
ATTN: H. Logston

EOS Technologies, Inc
ATTN: B. Gabbard
ATTN: W. LeLevier

General Electric Co
ATTN: A. Steinmayer
ATTN: C. Zierdt
ATTN: E. Cross
ATTN: R. Juner

General Electric Co
ATTN: G. Millman

General Research Corp
ATTN: B. Bennett

GTE Government Systems Corp
ATTN: R. Steinhoff

Honeywell, Inc
ATTN: G. Terry, Avionics Dept

Horizons Technology, Inc
ATTN: R. Kruger

HSS, Inc
ATTN: D. Hansen

IBM, Corp
ATTN: H. Ulander

Institute for Defense Analyses
ATTN: E. Bauer
ATTN: H. Wolfhard
ATTN: J. Aein

JAYCOR
ATTN: J. Sperling

JAYCOR
ATTN: H. Dickinson

M/A Com Linkabit, Inc
ATTN: A. Viterbi
ATTN: H. van Trees
ATTN: I. Jacobs

DEPARTMENT OF DEFENSE CONTRACTORS (Continued)

Johns Hopkins University
ATTN: C. Meng
ATTN: J. Phillips
ATTN: J. Newland
ATTN: K. Potocki
ATTN: R. Stokes
ATTN: T. Evans

Kaman Sciences Corp
ATTN: E. Conrad

Kaman Tempo
ATTN: B. Gambill
ATTN: DASIAC

Kaman Tempo
ATTN: DASIAC

Litton Systems, Inc
ATTN: B. Zimmer

Lockheed Missiles & Space Co, Inc
ATTN: J. Kumer
ATTN: R. Sears

Lockheed Missiles & Space Co, Inc
2 cys ATTN: D. Churchill, Dept 62-A1

M I T Lincoln Lab
ATTN: D. Towle
ATTN: I. Kupiec

Magnavox Govt & Indus Electronics Co
ATTN: G. White

Maxim Technologies, Inc
ATTN: J. Marshall
ATTN: R. Morganstern

McDonnell Douglas Corp
ATTN: W. Olson

Meteor Communications Corp
ATTN: R. Leader

Mission Research Corp
ATTN: B. William
ATTN: C. Lauer
ATTN: D. Knepp
ATTN: F. Fajen
ATTN: F. Guigliano
ATTN: G. McCartor
ATTN: R. Bigoni
ATTN: R. Bogusch
ATTN: R. Dana
ATTN: R. Hendrick
ATTN: S. Gutsche
ATTN: Tech Lib

Mission Research Corp
2 cys ATTN: D. Knepp
2 cys ATTN: W. Bradford

Mitre Corp
ATTN: A. Kymmel
ATTN: C. Callahan

Pacific-Sierra Research Corp
ATTN: E. Giller

DEPARTMENT OF DEFENSE CONTRACTORS (Continued)

Mitre Corp
ATTN: M. Horrocks
ATTN: W. Foster
ATTN: W. Hall

Pacific-Sierra Research Corp
ATTN: E. Fields, Jr.
ATTN: F. Thomas
ATTN: H. Brode, Chairman SAGE

Pacifica Technology
ATTN: E. Giller

Pennsylvania State University
ATTN: Ionospheric Research Lab

Photometrics, Inc
ATTN: I. Kofsky

Physical Dynamics, Inc
ATTN: E. Fremouw

Physical Research, Inc
ATTN: R. Deliberis
ATTN: T. Stephens

Physical Research, Inc
ATTN: J. Devore
ATTN: J. Thompson
ATTN: W. Schlueter

R & D Associates
ATTN: B. Moller
ATTN: C. Greifinger
ATTN: F. Gilmore
ATTN: G. StCyr
ATTN: H. Ory
ATTN: M. Gantsweg
ATTN: M. Grover
ATTN: P. Haas
ATTN: R. Turco
ATTN: W. Karzas
ATTN: W. Wright

R & D Associates
ATTN: B. Yoon

Rand Corp
ATTN: C. Crain
ATTN: E. Bedrozian
ATTN: M. Grover
ATTN: P. Davis

Rand Corp
ATTN: B. Bennett

Riverside Research Institute
ATTN: V. Trapani

Rockwell International Corp
ATTN: R. Buckner

Rockwell International Corp
ATTN: S. Quilici

Science Applications Intl Corp
ATTN: C. Smith
ATTN: D. Hamlin
ATTN: E. Straker
ATTN: L. Linson

DEPARTMENT OF DEFENSE CONTRACTORS (Continued)

Science Applications Intl Corp
ATTN: M. Cross

SRI International
ATTN: A. Burns
ATTN: C. Rino
ATTN: D. Nielson
ATTN: G. Price
ATTN: G. Smith
ATTN: J. Petricéks
ATTN: M. Baron
ATTN: R. Leadabrand
ATTN: R. Livingston
ATTN: R. Tsunoda
ATTN: W. Chesnut
ATTN: W. Jaye

Stewart Radiance Laboratory
ATTN: R. Huppi

DEPARTMENT OF DEFENSE CONTRACTORS (Continued)

Swerling, Manasse & Smith, Inc
ATTN: R. Manasse

Toyon Research Corp
ATTN: J. Garbarino
ATTN: J. Ise

TRW Electronics & Defense Sector
ATTN: R. Plebuch, 134/8085

Utah State University
ATTN: A.Steed
ATTN: D. Burt
ATTN: K. Baker, Dir Atmos & Space Sci
ATTN: L. Jensen, Elec Eng Dept

VisiDyne, Inc
ATTN: J. Carpenter

END

FILMED

5-86

DTIC